

Interface Resistances in Sputtered Pd/Pt CPP-MR Multilayers

S. Olson, J. Bass, W. Pratt, and R. Loloee

Introduction

The study of Giant Magnetoresistance (GMR) in magnetic multilayers is important not only in scientific fields, but also for technology because of its multiple practical applications, including read-heads for computer hard drives. In this project, current perpendicular to plane (CPP) Giant Magnetoresistance is utilized to study multilayer interface properties. This paper gives a brief overview of the creation and measurement of CPP-MR samples, compares the interface resistance of palladium-copper multilayer samples to the interface resistance $2AR_{\text{Pd/Cu}} = 0.9 \pm 0.1 \text{ f}\Omega\text{m}^2$ of previously sputtered palladium-copper exchange-bias spin valve samples [1], and uses sputtered palladium-platinum multilayer and palladium-platinum exchange-bias spin valve samples to study the resistance's dependence on the number of interfaces and thereby obtain a value for the specific resistance of a single palladium-platinum interface. It has been previously shown that the interface resistances of sputtered samples with multilayers composed of two elements with the same lattice parameters agree with no-free-parameter calculations for 'clean-and-perfect' interfaces and 50%-50% alloy interfaces. However, the interface resistances for sputtered samples whose multilayers are made of two elements that have different lattice parameters do not agree as well and the theoretical calculations are less reliable. Therefore, new multilayers whose elements have the same lattice parameters (palladium and platinum) have been sputtered in order to provide experimental results for future no-free-parameter calculations.

Procedure and Theory

Both spin valve and non-spin valve samples are produced by sputtering. Sputtering is the process of removing material from a solid target composed of a single element or alloy by

energetic ion bombardment in order to coat a substrate with the sputtered target material. The chamber in which the targets are placed is pumped down to a controlled pressure of $\sim 10^{-8}$ Torr. Argon gas is then introduced into the chamber, bringing the pressure up to 2×10^{-3} Torr. The argon is then ignited into plasma. A magnetron, involving perpendicular electric and magnetic fields, is then used to contain the plasma of positive Argon ions in the proximity of each target. These highly energetic ions accelerate towards the negatively charged target. When they strike the target, the energy transfer tears atoms off of the target surface. Some of the ejected target ions adhere to the substrate, creating a layer of target material. Collisions between the argon and the target create a cloud of target material, which helps to ensure a uniform deposition rate. Through monitoring the deposition rate, it is possible to control the thickness of the layer sputtered on the substrate. Sputtering one layer at a time until the desired geometry is completed creates the multilayered samples.

Two different series of the simple, non-spin valve samples have been created. The geometry for each of these is a 150 nm thick strip of niobium, then a 6 nm layer of cobalt, followed by a multilayer of alternating equal layers of two non-magnetic materials, another 6 nm layer of cobalt, and a second 150 nm strip of niobium. While the number and thickness of the individual layers varies from sample to sample, the total thickness and the amount of each material remains constant in all the samples. The first set of samples contained multilayers composed of palladium and copper and the second set contained multilayers of Palladium and Platinum. The sample geometry is shown graphically in figure 1. Figure 1 is not to scale, but is depicted in a way that stresses the geometry of the sample.

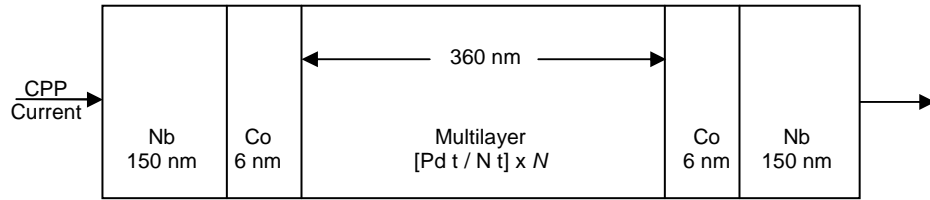


FIGURE 1. Geometry of simple, non-spin valve sample.

N represents the second element used to construct the multilayer, which is Cu in the first series and Pt in the second. The variable t is the thickness of each individual layer. The individual layer thicknesses for the Pd and Cu, or Pd and Pt, are equal. The script N is the total number of individual layers of each element. A typical sample, described as [Pd 18/Cu 18] x 10, has ten layers of Pd, each 18 nm thick, alternated with 10 layers of Cu 18 nm thick to create a total of 20 layers, 19 Pd/Cu interfaces and a total multilayer thickness of 360 nm. Again, it is important to note that t and N vary accordingly in each sample to keep the total multilayer thickness always 360 nm. Of the 360 nm, each sample has 180 nm of Pd and 180 nm of N . Since the amount of material in each sample is constant, only the number of interfaces is varied. This makes it possible to study at which point the layer thickness becomes so small that the multilayer is no longer a series of discernable layers of Pd and N , but becomes an alloy of Pd and N . At this point, the layer thickness t is no longer larger than the thickness of the Pd/ N interfaces and the entire sample, in effect, becomes a uniform alloy.

To measure the resistance, the sample is dipped into a dewar of liquid helium, which lowers the temperature of the sample to 4.2K. Nb ($T_C = 9.25$ K) is superconducting at 4.2 K. Because the Nb strips are superconducting and the surface area of the crossed Nb strips (~1.2mm) is much larger than the distance between each Nb strip (372nm), there is a uniform current density throughout the area A , shown in figure 3. The thin ferromagnetic Co layers protect the multilayer from the proximity effect with the superconducting Nb, which would

otherwise turn the multilayer superconducting. The resistances of the non-spin valve samples are measured only at a few fields ranging from 1000G to -1000G to check that these resistances are not magnetic field dependent.

The geometry for an exchange biased spin valve (EBSV) sample is much different from that of the non-spin valve sample. As shown in figure 2, the EBSV geometry is relatively complex.

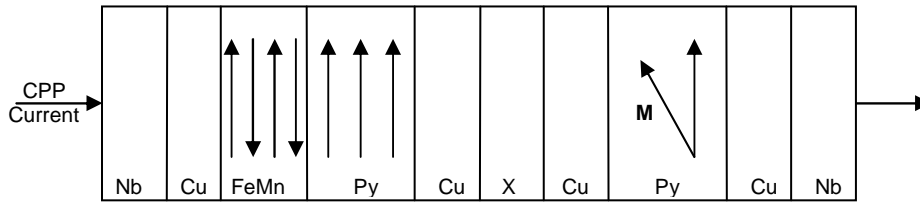


FIGURE 2. Geometry of EBSV sample.

As with figure 1, figure 2 is also not to scale to stress the geometry. The EBSV geometry involves a 150 nm thick strip of Nb, a 10 nm thick spacing layer of Cu, an 8 nm thick layer of FeMn, a 24 nm thick layer of permalloy (Py) which is the alloy $\text{Ni}_{84}\text{Fe}_{16}$, another 10 nm thick layer of Cu, the multilayer represented here as X is $[\text{Pd } 3\text{nm}/\text{Pt } 3\text{nm}] \times N$, another 10 nm layer of Cu, 24 nm layer of Py, 10 nm layer of Cu and the second 150 nm thick Nb strip. In the case of the EBSV, the individual layer thicknesses remain constant (3 nm) while the number of layers, N , varies. As N increases, more layers are added, increasing not only the number of interfaces, but also the amount of material in each multilayer.

Exchange bias pinning is the process in which the magnetic dipole moment of a ferromagnetic layer adjacent to an anti-ferromagnetic layer is pinned in a certain direction. This is accomplished by heating the sample, then cooling it in the presence of a magnetic field. In the EBSV samples, FeMn is anti-ferromagnetic and the Py layers are ferromagnetic. Figure 2 depicts the initial state of the FeMn and Py layers in the sample. Because the Py layer adjacent

to the FeMn layer is pinned, a considerably higher external magnetic field is required to flip the moment of the pinned Py layer than that of the unpinned Py layer.

The sample geometry is shown in figure 3. The circular multilayer is sandwiched between the crossed Nb strips, each ~ 1.1 mm wide.

To measure the GMR, the sample is dipped into a dewar of liquid helium and then placed in an external magnetic field parallel to the direction of the magnetization of the pinned F layer. The superconducting Nb strips ensure a uniform current density over the area $A \sim 1.2\text{mm}^2$. An external magnetic field, in the plane of the layers and along the pinning axis, is varied from negative to positive and back again, producing changes in resistance R , as illustrated in figure 4 for an EBSV with no insert. R varies from $R(P) \sim 13\text{n}\Omega$ to $R(AP) \sim 15\text{n}\Omega$, giving a maximum change in resistance $\Delta R = R(AP) - R(P) \approx 2\text{ n}\Omega$. Details are given in the caption of figure 4.

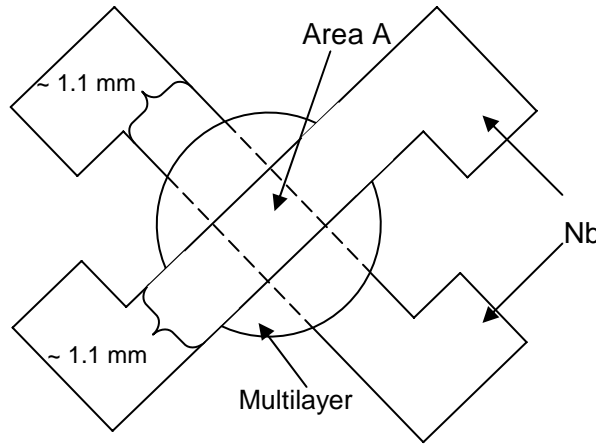


FIGURE 3. Geometry of CPP sample.

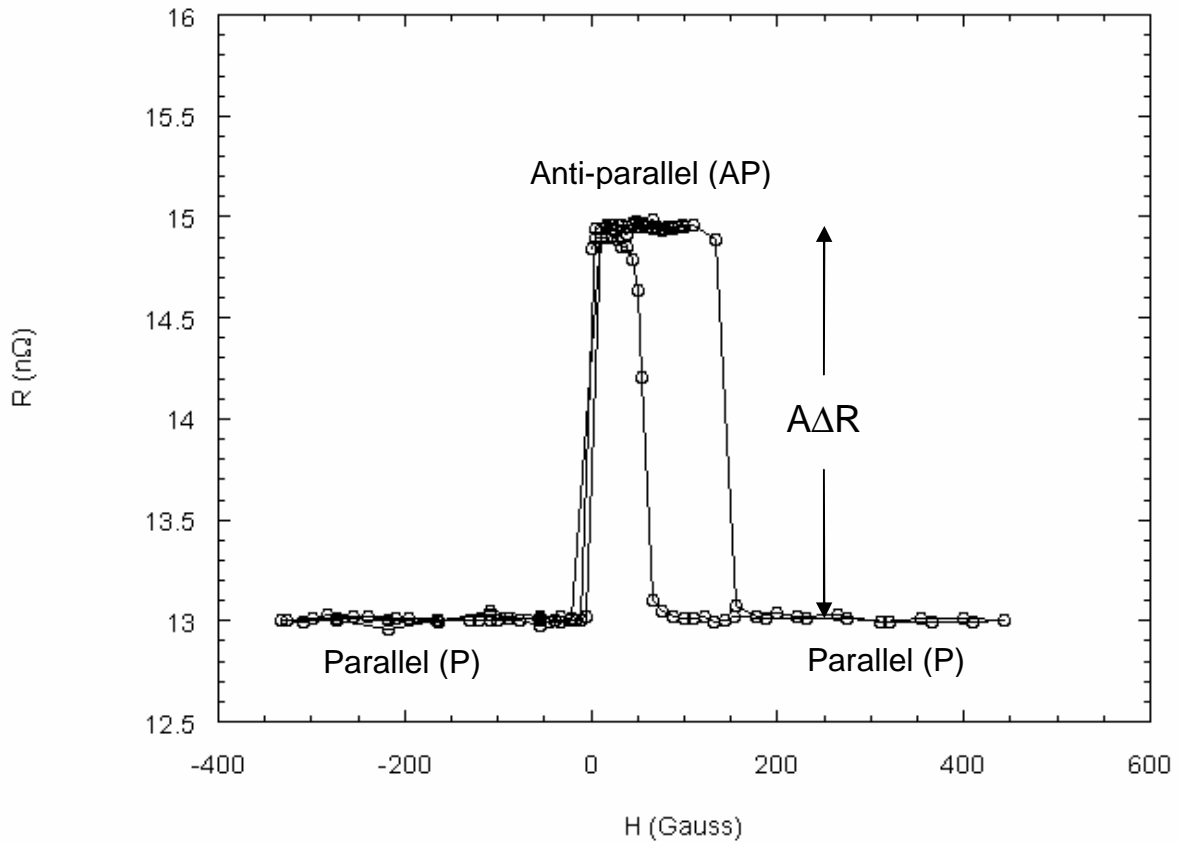


FIGURE 4. Graph of resistance (R) vs external magnetic field (H). Here the GMR is easily seen. This EBSV Pd/Pt sample has $N=0$. The magnetic field starts at -50 Gauss, decreases to -300 Gauss, which puts the Py layers in a parallel (P) state, increases to 100 Gauss, flipping the unpinned Py layer and changing the sample to anti-parallel (AP), decreases to -300 Gauss again, flipping the unpinned Py layer back, returning the sample to P, and completing a minor loop. Then the field increases to 400 Gauss, flipping first the unpinned Py layer (AP), then the pinned Py layer (P), then decreases to 0 Gauss, again flipping the pinned Py layer (AP) and completing the major loop.

While the sample is at 4.2 K and in the presence of the magnetic field, a current of 100 mA is run through the sample perpendicular to the plane of the layers via the superconducting Nb strips. This is called the current perpendicular to plane (CPP) method and its direction is depicted in figures 1 and 2. CPP measurements require four contacts on the sample; two for current and two for voltage. By placing the voltage and current contacts on the superconducting Nb strips, the current is forced to travel through the $\sim 1.2\text{mm}^2$ area of the multilayer

perpendicular to the plane of the sample. The very small values of R are measured with a Superconducting Quantum Interference Device (SQUID)-based null detector [2]. The specific resistance, AR (area times resistance), rather than R , is the intrinsic quantity for the sample. By using the CPP method, the current passes through each individual layer of the sample in series, and, if electrons do not flip their spins in transit, it has been shown that AR should be given by the straightforward two-current series resistor (2CSR) model [3,4], which will be described below.

If electron spins are flipped as they pass through the N layers in the middle of an EBSV, Pratt has used the theory of Valet and Fert [4] to show that $A\Delta R$ decreases as $\exp(-l_{sf}^N)$ due to switching within a single layer, or as $\exp(-2\delta_{N1/N2}N)$ due to flipping at $2N$ interfaces. This result is used to derive $\delta_{Pd/Pt}$ from the data [5].

By measuring the specific resistance of the entire sample and calculating values for the resistances of the individual layers, the 2CSR model allows for calculations of the interface resistances. The resistance of an individual layer or interface can be obtained through the simple relationship

$$R = \rho t/A \text{ or } AR = \rho t \quad (1)$$

where R is the resistance, ρ the resistivity, t the thickness of the layer, and A the area of the sample. $AR_{N1/N2}$ describes the interface resistances and ρ_{NtN} describes the individual layers of the sample.

The resistivities of Pd, Nb, Cu, Co, and Pt were all measured by sputtering a thin film of an element or alloy and utilizing the Van der Pauw method. All of the resistivities agree with previous measurements with the exception of Pt, which was found to be somewhat lower.

However, three separate CIP films of Pt were sputtered on two separate occasions and all were

found to be in agreement with each other. The values of the high and low temperature resistivities are listed in Table I.

The 2CSR expression for the simple, non-spin valve Pd/Pt samples are described by

$$AR_T = 2AR_{S/Co} + 2\rho_{Co}t_{Co} + AR_{Co/Pd} + AR_{Pt/Co} + \rho_{Pd}(180nm) + \rho_{Pt}(180nm) + 2NAR_{Pd/Pt} \quad (2)$$

where AR_T is the total specific resistance of the sample. The values on the right side of the equation are the interface specific resistances and the individual layer specific resistances. Every factor on the right side of the equation is a constant except the term $2NAR_{Pd/Pt}$. $2AR_{Pd/Pt}$ is the resistance of two Pd/Pt interfaces.

The more complex EBSV Pd/Pt samples are described by

$$AR_T = C + N\rho_{Pd}(3nm) + N\rho_{Pt}(3nm) + (2N-1)AR_{Pd/Pt} \quad (3)$$

where C is a constant that includes all the interface and layer resistances for layers outside the multilayer, which are constant for all samples.

Data and Analysis

Once the areas and resistances of the samples are measured, AR is graphed as a function of N . The plot of AR vs N produces a straight line, the slope of which is $2AR_{Pd/N}$ for simple non-spin valve samples and $2AR_{Pd/Pt} + \rho_{Pd}(3nm) + \rho_{Pt}(3nm)$ for EBSV Pd/Pt spin valve samples.

The graph of AR vs N for the Pd/Pt simple non-spin valve data gives the specific resistance of two Pd/Cu interfaces, $2AR_{Pd/Cu}$. The data in figure 5 are linear only up to $N \sim 120$, above which they slowly round off. This round off is presumably because as t decreases and N increases, the individual layers of the multilayer become less defined and the sample begins to resemble an alloy of Pd/Cu rather than a series of discrete individual layers of Pd and Cu. As such, AR values corresponding to $N > 120$ are excluded from the linear fit. The circles and squares, and their fits, in figure 5 are from the same Pd/Cu samples and use identical values of

the multilayer resistance. The only difference between the two is that the areas of the same samples were measured independently by two different people, once by Sam Olson and again by Huseyin Kurt. The average of these values produces the value $2AR_{Pd/Cu} = 0.74 \pm 0.1 \text{ f}\Omega\text{m}^2$ for the interface resistance of a Pd/Cu simple non-spin valve multilayer.

The plot of AR vs N for the Pd/Pt non-spin valve samples is one of the two graphs that supply the interface resistance for Pd/Pt multilayers. The graph is shown in figure 6. Similar to figure 5, the linear fit excludes AR values corresponding to $N > 120$. However, in the case of Pd/Pt, the saturation is not as prevalent as in the Pd/Cu data. As an alternative, forcing all the data to a linear fit, should give a lower bound estimate of $2AR_{Pd/Pt} \approx 0.25 \text{ f}\Omega\text{m}^2$. We thus estimate $2AR_{Pd/Pt} = 0.28 \text{ f}\Omega\text{m}^2 \pm 0.03 \text{ f}\Omega\text{m}^2$.

The EBSV Pd/Pt data plotted in figure 7 produces an alternative value for $2AR_{Pd/Pt}$ that can be compared with that of the non-spin valve data. Figure 7 depicts the graph of the average resistance, $AR_{AVG} = [AR(AP) - AR(P)]/2$, of the P and AP states for the EBSV samples as a function of N . As shown in equation 3, the slope of this graph is $2AR_{Pd/Pt} + \rho_{Pd}(3\text{nm}) + \rho_{Pt}(3\text{nm})$. Therefore, to obtain the Pd/Pt interface resistance $2AR_{Pd/Pt}$, it is necessary to subtract $\rho_{Pd}(3\text{nm})$ and $\rho_{Pt}(3\text{nm})$ from the slope. The measured values of the resistivities of Pd and Pt respectively are: $\rho_{Pd} = 4.5 \text{ }\mu\Omega\text{cm}$ and $\rho_{Pt} = 2.6 \text{ }\mu\Omega\text{cm}$. These values, when multiplied by the thickness $t = 3\text{nm}$, produces the resistances $R_{Pd} = 0.135 \text{ f}\Omega\text{m}^2$ and $R_{Pt} = 0.075 \text{ f}\Omega\text{m}^2$. These two values are then subtracted from $0.39 \text{ f}\Omega\text{m}^2 \pm 0.12 \text{ f}\Omega\text{m}^2$ to obtain a value of $0.18 \text{ f}\Omega\text{m}^2 \pm 0.14 \text{ f}\Omega\text{m}^2$ for $2AR_{Pd/Pt}$.

Analysis of GMR in EBSV samples also lets us derive $\delta_{Pt/Pd}$ by plotting $A\Delta R$ vs N , as shown in figure 8. The slope of the plot of $A\Delta R$ vs N for Pd/Pt EBSV is closer to the slope of ΔR vs N for Pd/Cu EBSV than that of the $A\Delta R$ vs N for Pt/Cu [1]. We estimate $\delta_{Pd/Pt} \sim 0.2$.

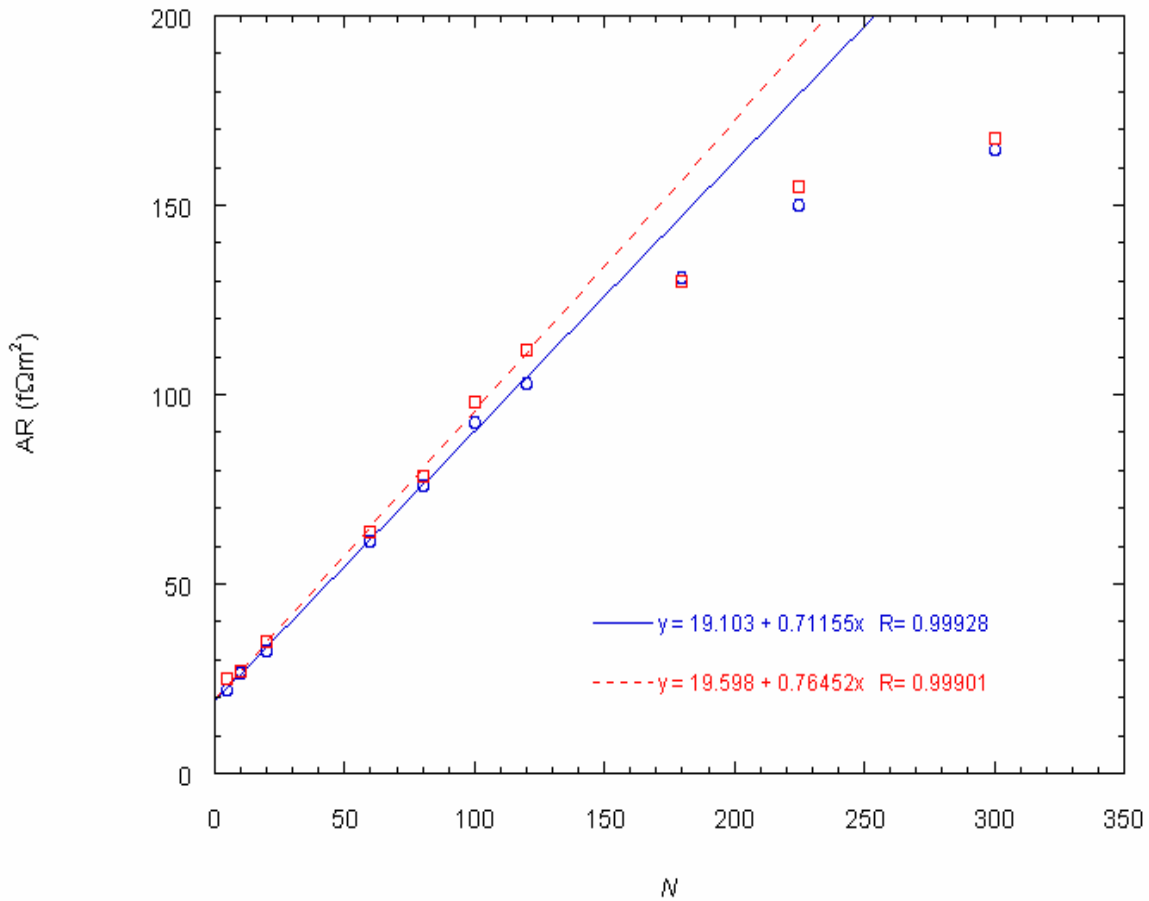


FIGURE 5. Graph of AR vs N for Pd/Cu. The two plots shown are the same samples and the same resistance values, but the areas were measured separately by two different people. The square points with the dashed fit line show the area measurements done by Huseyin Kurt and the circle points with the solid fit line were measured by Sam Olson. The slope formula for each fit line is shown, displaying the y intercept and the slope of each line. The linear fits exclude all AR values corresponding to $N > 120$, where the saturation is argued to initiate.

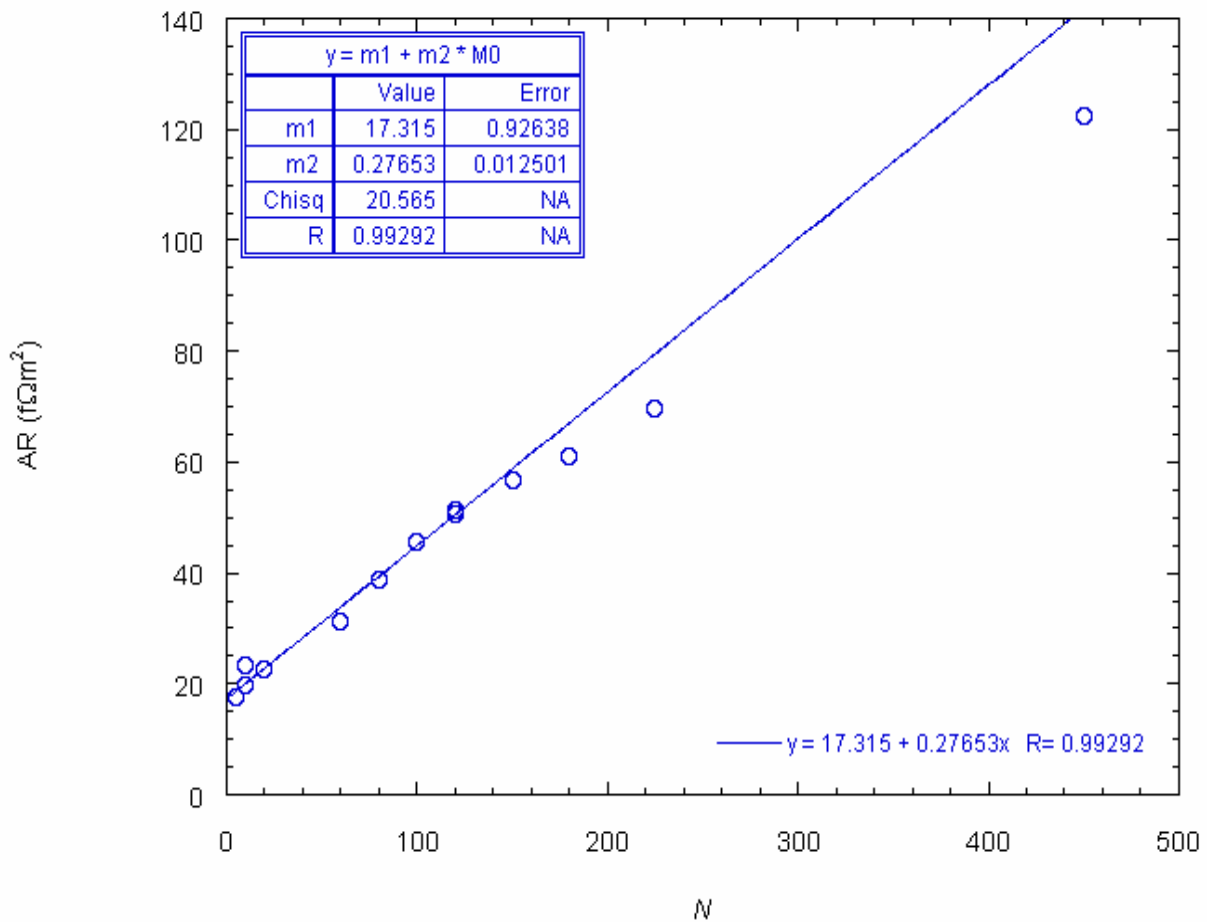


FIGURE 6. Graph for AR vs N for Pd/Pt non-spin valve samples. This plot is shown not only with the equation for the straight line, but also with a text box. The top two rows of the text box hold the important information: the values next to “m1” correspond to the y-intercept value and uncertainty and the values next to “m2” correspond to the slope and its uncertainty.

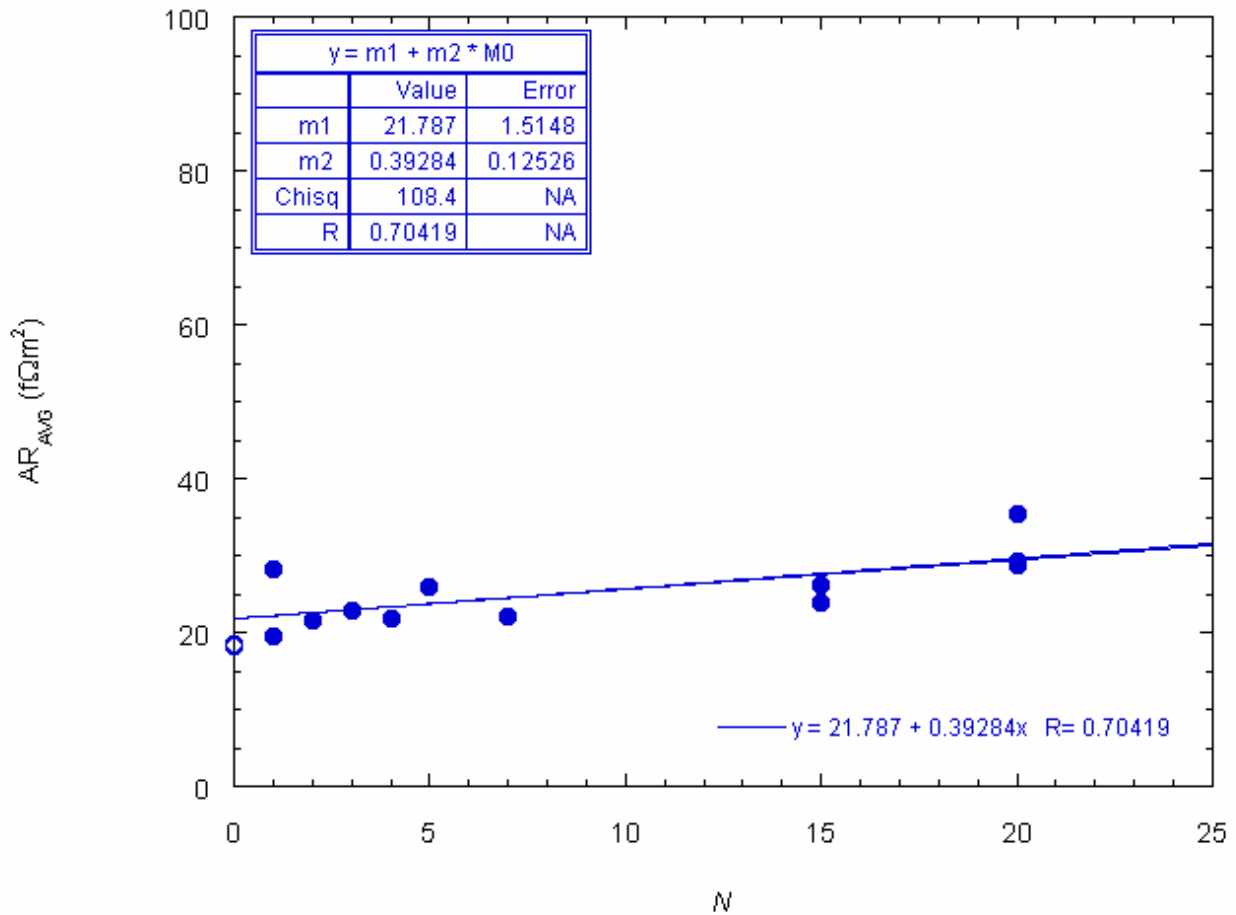


FIGURE 7. Graph of AR_{AVG} vs N for Pd/Pt EBSV samples. All points are plotted as filled in circles except $N=0$ because a correction factor is needed before the $N=0$ points can be included in the fit. The correction factor comes about because all of the points except $N=0$ receive extra resistance from the outer Cu/Pd and Pd/Cu interfaces. At $N=0$, these interfaces are not present because there is no Pd/Pt multilayer. The linear fit pictured here excludes the $N=0$ points. Again, in the enclosed table, “m1” corresponds to the value and uncertainty of the y intercept and “m2” corresponds to the value and uncertainty of the slope.

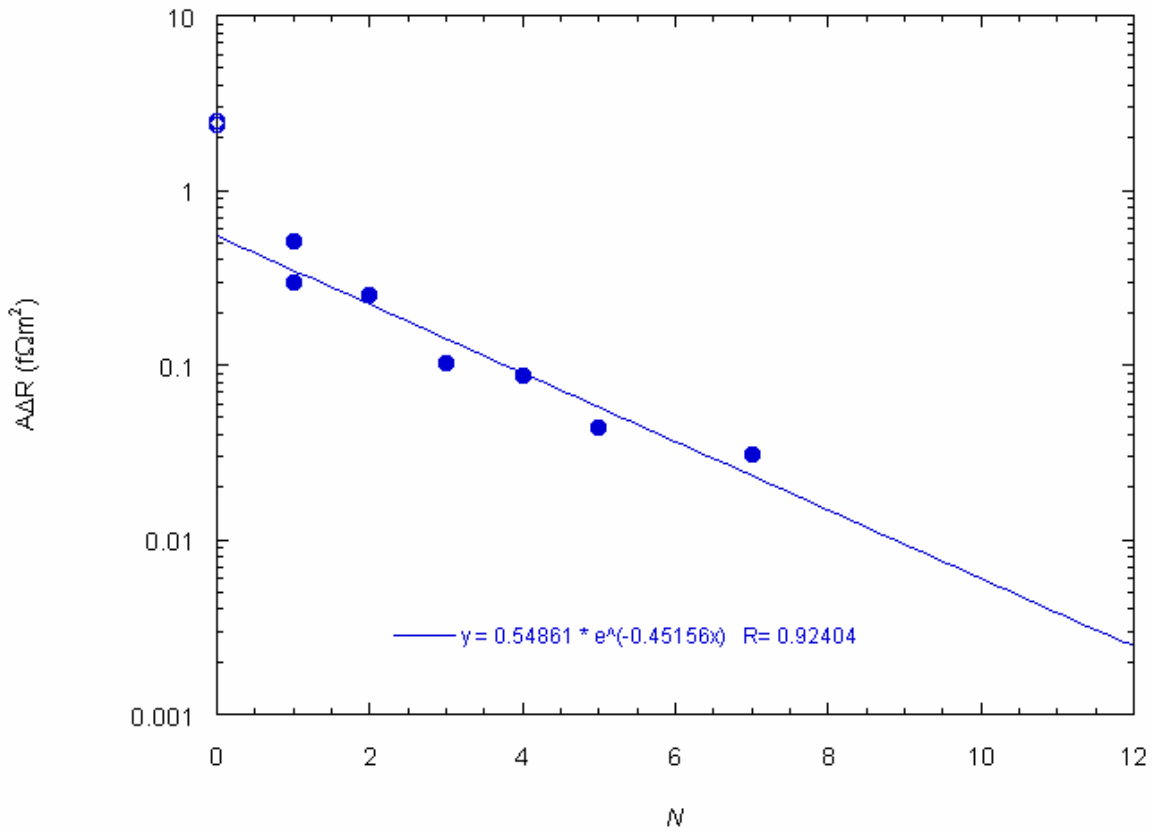


FIGURE 8. Graph of $A\Delta R$ vs N for Pd/Pt EBSV samples. As with figure 7, all points are plotted as filled in circles except $N=0$ because a correction factor is needed before the $N=0$ points can be included in the fit. The correction factor comes about because the all points except $N=0$ receive extra resistance and spin-flipping from the outer Cu/Pd and Pt/Cu interfaces. At $N=0$, these interfaces are not present because there is no Pd/Pt multilayer. The exponential fit pictured here excludes the $N=0$ points.

Table I.

	Pd	Co	Cu	Pt	Nb
Room Temperature	15.5	10.7	2.6	13.9	17.2
4.2 K	4.5	4.2	0.7	2.6	4.2*

TABLE I. Measured Resistivities of sputtered 200 nm thick films of the elements listed. All measurements, with the exception of the low temperature Nb, were performed at room temperature and 4.2 K. The resistivities are shown in units of $\mu\Omega\text{cm}$.

* The low temperature Nb measurement was conducted at a temperature of 12.0 K because Nb is superconducting below 9 K.

Conclusions

The sputtering procedures, processes for measuring MR, GMR and the resistivities, and the 2CSR model for analysis are by now, well established.

The interface resistance of Pd/Cu for simple non-spin valve samples is $2AR_{\text{Pd/Cu}} = 0.74 \pm 0.1 \text{ f}\Omega\text{m}^2$. While this value is lower than $0.9 \pm 0.1 \text{ f}\Omega\text{m}^2$, the previously measured interface resistance of an EBSV Pd/Cu sample, the two values overlap within their mutual uncertainties.

The value of $2AR_{\text{Pd/Pt}}$ provided by the non-spin valve samples is $0.28 \text{ f}\Omega\text{m}^2 \pm 0.03 \text{ f}\Omega\text{m}^2$. The value of $2AR_{\text{Pd/Pt}}$ obtained through measurement and analysis of the EBSV samples is $0.18 \text{ f}\Omega\text{m}^2 \pm .14 \text{ f}\Omega\text{m}^2$. These values of $2AR_{\text{Pd/Pt}}$ have been produced by the two independent methods and overlap within their mutual uncertainties. From the data measured here, an initial estimate of $0.25 \text{ f}\Omega\text{m}^2 \pm 0.07 \text{ f}\Omega\text{m}^2$ for the value of $2AR_{\text{Pd/Pt}}$ is offered as a value to which future calculations might be compared. We also estimate $\delta_{\text{Pd/Pt}} \sim 0.2$.

References

1. H. Kurt *et al.*, Appl. Phys. Lett. **81**, 4787 (2002).
2. S. F. Lee *et al.*, Phys. Rev. **B52**, 15426 (1995).
3. S. F. Lee *et al.*, J. Magn. Magn. Mat. **118**, L1 (1993).
4. T. Valet and A. Fert, Phys. Rev. **B48**, 7099 (1993).
5. W. Park *et al.*, Phys. Rev. **B62**, 1178 (2000).